

# $\mathcal{PT}$ symmetry breaking in photonic waveguides with competing gain rates

P. A. Kalozoumis,<sup>1</sup> C. V. Morfonios,<sup>2</sup> F. K. Diakonos,<sup>1</sup> and P. Schmelcher<sup>2,3</sup>

<sup>1</sup>*Department of Physics, University of Athens, GR-15771 Athens, Greece*

<sup>2</sup>*Zentrum für Optische Quantentechnologien, Universität Hamburg,  
Luruper Chaussee 149, 22761 Hamburg, Germany*

<sup>3</sup>*The Hamburg Centre for Ultrafast Imaging, Universität Hamburg,  
Luruper Chaussee 149, 22761 Hamburg, Germany*

(Dated: April 25, 2022)

We consider a discrete  $\mathcal{PT}$  symmetric quadrimer optical structure with two competing gain parameters. The existence of the additional loss/gain rate has a major impact on the phase diagram of the system leading to multiple transitions, not only between the unbroken and a broken phase, but also between broken phases with distinct light propagation properties. The  $\mathcal{PT}$ -unbroken phase is shown to be characterized by the vanishing of a symmetry-adapted nonlocal current  $Q$ , whose site-average behaves as a natural order parameter across the spontaneous symmetry breaking transition. Utilizing the quadrimer as a unit cell of a uniform lattice, we investigate how the corresponding band structure and the attendant beam dynamics in large waveguide arrays are affected by the existence of the second loss/gain parameter. The enriched band structure landscape yields the possibility to control the propagation length of a beam before divergence when the system resides in the broken  $\mathcal{PT}$  phase.

PACS numbers: 42.25.Bs, 42.82.Et, 78.67.Pt, 78.67.Bf

## I. INTRODUCTION

The concept of non-Hermitian systems with  $\mathcal{PT}$ -symmetry has developed into a rapidly evolving research field in contemporary physics, extending from quantum mechanics [1] and field theory [2] to systems with topological states [3–5], optics [6–11] and acoustics [12–14]. In the seminal work of Bender *et al* [15] it was demonstrated that a class of non-Hermitian Hamiltonians can possess, for certain parametric ranges, entirely real eigenvalue spectra, indicating the unbroken  $\mathcal{PT}$  symmetric phase where both the Hamiltonian  $\hat{\mathcal{H}}$  and the  $\hat{\mathcal{PT}}$  operator share the same set of eigenvectors. On the other hand, by varying the parameter which determines the amount of loss and gain, a spontaneous symmetry breaking occurs suggesting that even though the operators  $\hat{\mathcal{H}}$  and  $\hat{\mathcal{PT}}$  still commute,  $[\hat{\mathcal{H}}, \hat{\mathcal{PT}}] = 0$ , they possess different eigenvectors, rendering the eigenvalue spectrum complex.

Since then, the progress in the field of  $\mathcal{PT}$  symmetric systems was enormously impelled by the adaptation of the corresponding concepts in optical structures and the experimental realization of the spontaneous  $\mathcal{PT}$  symmetry breaking [16, 17]. The link between wave optics and quantum mechanics stems from the isomorphism of the paraxial Helmholtz approximation to the time-dependent Schrödinger equation, where the axial variation along the  $z$ -axis (propagation axis) corresponds to the time evolution in the quantum mechanical case. In the realm of discrete optics, one-dimensional  $\mathcal{PT}$ -symmetric photonic waveguide systems have been associated with appealing phenomena such as double refraction [7], power oscillations [16] and non-reciprocal diffraction [18]. In the presence of nonlinearity, unidirectional [19] and asymmetric [20, 21] wave propagation have been observed. Moreover, in extended  $\mathcal{PT}$  symmetric lattices Bloch oscillations are feasible [22] whereas also universality in beam dynamics has been reported [23]. Apart from discrete

bounded systems, also continuous  $\mathcal{PT}$ -symmetric multilayered scattering devices have been addressed. Similarly to the discrete case, the usual pathway towards the study of such systems is to consider refraction index landscapes obeying the symmetry  $n(x) = n^*(-x)$  which corresponds to balanced gain and loss [24]. This class of  $\mathcal{PT}$  symmetric setups yield intriguing properties such as CPA-laser points [22, 25], anisotropic transmission resonances [26] and  $\mathcal{PT}$  symmetry induced, spatially invariant currents [27]. Recently, the bounded and unbounded cases were linked in Ref. [28].

In the present work we focus on the coexistence of two different gain rates in discrete non-Hermitian photonic systems with global  $\mathcal{PT}$  symmetry. Motivated from the intriguing properties of oligomers [20, 29, 30], i.e. single  $\mathcal{PT}$  dimers [19, 31], trimers [32] and quadrimers [33–37], we investigate the behaviour of a linear, discrete  $\mathcal{PT}$ -symmetric optical quadrimer, where the loss/gain rate in the two inner waveguides differs from the loss/gain rate of the two outer waveguides. We find that the existence of two different loss/gain rates induces a rich phase diagram with transitions, not only between the unbroken and broken phases, but also between  $\mathcal{PT}$  broken phases. Compared to the usual case of single bifurcation phase diagrams, this one offers the possibility to have parametric regions of qualitatively different phases of broken  $\mathcal{PT}$  symmetry which are distinguishable through the associated light propagation properties. We also examine the existence of a  $\mathcal{PT}$  symmetry induced, nonlocal current-like quantity  $Q$  which is spatially constant and zero in the unbroken phase. It was recently shown [27] that the continuous scattering version of  $Q$  provides a systematic way to describe the transition from the broken ( $Q \neq 0$ ) to the unbroken ( $Q = 0$ ) phase, allowing for the generalization of the phase diagram from  $S$ -matrix eigenstates [25] to arbitrary scattering states. In the case of a (discrete) bounded system, the imaginary part of eigenener-

gies leads to non-constancy of  $Q$ , whereby we here use its site-average  $\langle Q \rangle$  to describe the transition between the broken and unbroken  $\mathcal{PT}$  phases. The results presented in this work along with the results of Ref. [27] suggest that  $\langle Q \rangle$  plays the role of a natural order parameter for the general class of  $\mathcal{PT}$  symmetric systems, allowing a unified description of the transition both in scattering and in bounded settings. Finally, using the quadrimer as a unit cell we find the band structure of the corresponding periodic system. Using a Bloch mode analysis we associate the light propagation properties in extended waveguide arrays to the band structure landscape, emphasizing on propagation distances a wavepacket can travel, while the system resides in the  $\mathcal{PT}$  broken phase.

The paper is organized as follows: In Sec. II we introduce the setup and deduce the corresponding phase diagram. In Sec. III we discuss the role of the  $\mathcal{PT}$  symmetry induced current  $Q$  in the description of the symmetry breaking in the general class of  $\mathcal{PT}$  systems. In Sec. IV we investigate the light propagation properties of the quadrimer in each eigenvalue region of the phase diagram. Special attention is paid to the vicinity of specific exceptional points (EP). Finally, in Sec. V we use the quadrimer as the unit cell and study the band structure of the corresponding periodic system. In Sec. VI we summarize our results.

## II. DESCRIPTION OF THE MODEL

$\mathcal{PT}$  symmetry signifies the existence of a parametric region where the eigenvalue spectrum becomes real. The well-known  $\mathcal{PT}$ -symmetric dimer [31] constitutes a prototype model which, below a critical value  $\gamma_c$  of the loss/gain rate which acts as the tuning parameter, exhibits a purely real eigenvalue spectrum, whereas above  $\gamma_c$  the spectrum becomes imaginary.

Here, we consider a  $\mathcal{PT}$ -symmetric optical quadrimer comprised of four photonic waveguides as shown in Fig. 1. The on-site potentials have the form  $v_m = n_m \pm i\gamma_m$ , with  $n_m$  being the refraction index of the  $m$ -th waveguide and  $\gamma_m$  the corresponding loss/gain rate. We assume then that the quadrimer exhibits *two different* competing loss/gain rates  $\gamma, \tilde{\gamma}$  with  $\gamma_1 = \gamma_4 = \gamma, \gamma_2 = \gamma_3 = \tilde{\gamma}$  arranged in order that the  $\mathcal{PT}$  symmetry of the setup is globally fulfilled. The addition of a second loss/gain rate has been discussed in a different context in Ref. [33], where the focus was on nonlinear modes in finite  $\mathcal{PT}$  symmetric systems. Also, we assume equal refraction indices  $n_m = n$ . According to coupled mode theory, the propagation of the wave field along the  $z$ -axis is described by the following set of four equations ( $m = 1, 2, 3, 4$ ),

$$i \frac{d\psi_m}{dz} = v_m \psi_m + h_{m,m+1} \psi_{m+1} + h_{m,m-1} \psi_{m-1}, \quad (1)$$

where  $v_m$  is the on-site potential and  $h_{m,m\pm 1}$  describes the hopping from the  $m$ -th waveguide to the  $(m \pm 1)$ -th. The system is bounded by setting  $h_0$  and  $h_5$  to zero. This set of equations can be written compactly in matrix

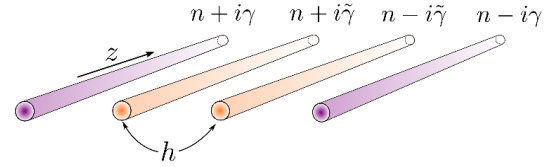


FIG. 1. (color online) Schematic of the setup, consisting of four waveguides with equal refraction indices  $n$ , uniform hoppings  $h$  and two competing loss/gain parameters  $\gamma, \tilde{\gamma}$ .

notation as

$$i \frac{d}{dz} |\Psi\rangle = \hat{\mathcal{H}} |\Psi\rangle, \quad (2)$$

with

$$\hat{\mathcal{H}} = \begin{pmatrix} v & h & 0 & 0 \\ h & \tilde{v} & h & 0 \\ 0 & h & \tilde{v}^* & h \\ 0 & 0 & h & v^* \end{pmatrix} ; \quad |\Psi\rangle = \begin{pmatrix} \psi_1 \\ \psi_2 \\ \psi_3 \\ \psi_4 \end{pmatrix}, \quad (3)$$

where  $v_1 = v, v_2 = \tilde{v}, v_3 = \tilde{v}^*, v_4 = v^*$  and  $h_{m,m\pm 1} = h$  (the star denotes complex conjugation).

The extension of the parameter space which follows the introduction of the additional tunable parameter  $\tilde{\gamma}$  has a significant impact on the behaviour of the system and particularly on the phase diagram. The diagonalization of the matrix  $\hat{\mathcal{H}}$  yields the following four energy eigenvalues:

$$\varepsilon_j = \pm \frac{1}{\sqrt{2}} \left( \sqrt{a \pm \sqrt{b}} + n \right) ; \quad j = 1, 2, 3, 4, \quad (4)$$

where

$$a = -(\gamma^2 + \tilde{\gamma}^2 - 3h^2), \\ b = (\gamma^2 - \tilde{\gamma}^2)^2 - 2(\gamma + \tilde{\gamma})(\gamma + 3\tilde{\gamma})h^2 + 5h^4,$$

the form of which is drastically affected by both  $\gamma$  and  $\tilde{\gamma}$ . In order to investigate the  $\mathcal{PT}$ -symmetry breaking, we employ Eq. (4) and search for the parametric space where the corresponding spectrum becomes real. Figure 2 (a), (b) illustrates the imaginary and real parts of the four (shifted) eigenvalues  $\bar{\varepsilon}_j = \sqrt{2}\varepsilon_j - n$  versus  $\tilde{\gamma}$ , respectively. The use of  $\bar{\varepsilon}_j$  aims to shift the real spectrum in order to become symmetric around  $\text{Re}[\bar{\varepsilon}_j] = 0$ , instead of  $\text{Re}[\varepsilon_j] = n$ . The other relevant parameters are kept fixed at values  $\gamma = 0.08, h = 0.1$  and  $n = 0.1$ . Notice that  $\tilde{\gamma}$  can take on negative values without affecting the  $\mathcal{PT}$  symmetry of the system, thus allowing for a variety of transitions between  $\mathcal{PT}$  broken and unbroken phases, generally not symmetric with respect to  $\tilde{\gamma} = 0$ . In the rest of our analysis all units are expressed in terms of the hopping rate  $h$  in order to render Eq. (1) dimensionless.

The phase diagram is characterized by six distinct eigenvalue regions (three on either side of  $\tilde{\gamma} = 0$ ), delimited by the dashed lines. Regions  $I$  and  $I'$  correspond to the unbroken  $\mathcal{PT}$  symmetric phase and exhibit a four-fold degeneracy of  $\text{Im}[\bar{\varepsilon}_j] = 0$ , indicating a real spectrum. The corresponding  $\text{Re}[\bar{\varepsilon}_j]$  are here nondegenerate

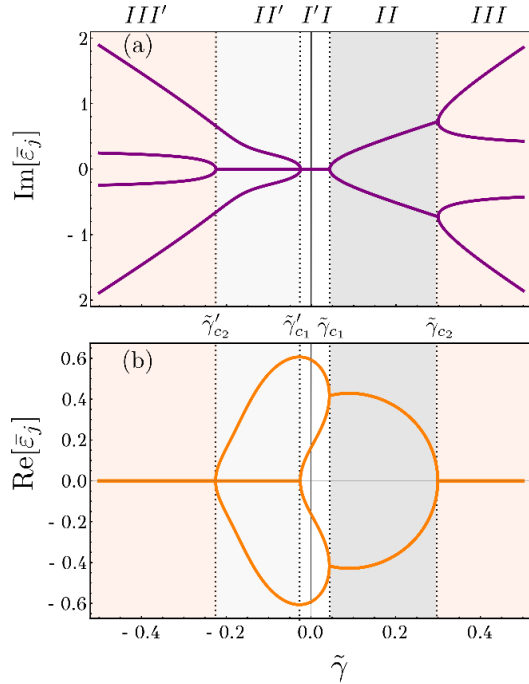


FIG. 2. (color online) (a) Imaginary part and (b) real part of the eigenvalue spectrum of the setup of Fig. 1 as a function of the loss/gain parameter  $\tilde{\gamma}$ . Dotted vertical lines indicate transition points  $\tilde{\gamma}_{c_i}$  ( $\tilde{\gamma}'_{c_i}$ ),  $i = 1, 2$ , between different  $\mathcal{PT}$  phases denoted by regions  $I, II, III$  ( $I', II', III'$ ) for  $\tilde{\gamma} > 0$  ( $\tilde{\gamma} < 0$ ). The region shadings highlight their qualitative difference: real ( $I, I'$ ), complex ( $II, II'$ , with distinct partial degeneracy) and imaginary ( $III, III'$ ) spectrum.

(regions  $I$  and  $I'$  in Fig. 2 (b)). At a critical value  $\tilde{\gamma}_{c_1}$ , the  $\text{Im}[\tilde{\varepsilon}_j]$  bifurcate, while the  $\text{Re}[\tilde{\varepsilon}_j]$  coalesce, into two doubly degenerate eigenvalues, indicating the transition from the  $\mathcal{PT}$ -symmetric phase to a broken phase with *complex* eigenvalue spectrum in region  $II$ . For  $\tilde{\gamma} < 0$ , another critical value  $\tilde{\gamma}'_{c_1}$  exists, also corresponding to a  $\mathcal{PT}$  symmetry breaking. Nonetheless, region  $II'$  is characterized by one doubly degenerate zero eigenvalue and two distinct complex eigenvalues, leading to qualitatively different wave propagation properties as compared to  $II$ , to be seen in Sec. IV. At larger  $|\tilde{\gamma}|$ , the  $\text{Im}[\tilde{\varepsilon}_j]$  further bifurcate at  $\tilde{\gamma}_{c_2}$  and  $\tilde{\gamma}'_{c_2}$ , with a purely imaginary spectrum in regions  $III$  and  $III'$ , respectively. Even though the light propagation properties in both those regions are similar, growing exponentially as in the  $\mathcal{PT}$ -symmetric dimer, the main difference lies in the transition to each phase: At  $\tilde{\gamma}_{c_2}$  it results from one bifurcation in each of the two complex branches in  $II$ , while at  $\tilde{\gamma}'_{c_2}$  the outer two imaginary parts continue smoothly from the branches in  $II'$ .

The rich phase diagram of the system with the three distinct types of broken phases ( $II, II', III/III'$ ) stems exclusively from the addition of the extra loss/gain parameter  $\tilde{\gamma}$ . Keeping the quadrimer structure and setting  $\tilde{\gamma} = \gamma$  or  $\tilde{\gamma} = -\gamma$ , results in a phase diagram with a single bifurcation from the  $\mathcal{PT}$  unbroken phase (real eigenvalues) to a  $\mathcal{PT}$  broken phase with complex eigenvalues.

Note also that by varying one of the loss/gain parameters it is possible to manipulate the width of the unbroken phase. To our knowledge, for linear oligomers, the departure from single bifurcation phase diagrams to more complex, as the one studied hereto, is possible only with the choice of adding an additional loss/gain rate. The addition of different hopping values or different refraction index values do not lead to multiple transition phase diagrams, retaining the single bifurcation pattern. Hence, the choice of different loss/gain parameters proposed here offers a tool to manipulate the phase diagram in a unique way and in turn to exploit the different propagation properties of each phase, as we shall see in the next section.

### III. $\mathcal{PT}$ SYMMETRY BREAKING AND NONLOCAL CURRENTS

In a sequence of recent works [27, 38–41] it was shown that discrete symmetries such as translation, reflection, and  $\mathcal{PT}$ -symmetry entail the emergence of nonlocal currents which are spatially invariant within domains which obey the corresponding symmetry. Such a nonlocal invariant provides a generic description of discrete symmetry breaking and additionally allows for the generalization of the Bloch and parity theorems for systems with broken translation and reflection symmetry, respectively [38]. These works referred exclusively to continuous scattering systems. Here, we extend this analysis to discrete systems with  $\mathcal{PT}$  symmetry and implement it on the proposed quadrimer. A generic theoretical analysis of discrete systems—both bounded and scattering—possessing global or local symmetries (including reflection and translation combined with time reversal) in terms of the corresponding nonlocal currents is presented in Ref. [42]. Here we will see how those currents can be employed to describe the spontaneous  $\mathcal{PT}$ -symmetry breaking in discrete bounded systems with global  $\mathcal{PT}$  symmetry. Substituting  $\psi_m = \alpha_m^{(j)} e^{i\varepsilon_j z}$ , we can write the close-coupling Eqs. (1) as

$$\varepsilon_j \alpha_m^{(j)} = v_m \alpha_m^{(j)} + h \left( \alpha_{m+1}^{(j)} + \alpha_{m-1}^{(j)} \right), \quad (5)$$

$$\varepsilon_j^* \alpha_{\bar{m}}^{*(j)} = v_{\bar{m}}^* \alpha_{\bar{m}}^{*(j)} + h \left( \alpha_{\bar{m}-1}^{*(j)} + \alpha_{\bar{m}+1}^{*(j)} \right) \quad (6)$$

for the  $\mathcal{PT}$  symmetry related sites  $m$  and  $\bar{m} = N+1-m$ , respectively, where  $N$  is the total number of waveguides. The mode  $\alpha^{(j)}$  corresponds to the  $j$ -th eigenvector (with eigenvalue  $\varepsilon_j$ ) of the matrix  $\mathcal{H}$  in Eq. (3). Every such eigenvector represents a light amplitude distribution across the  $x$ -direction whose intensity does not evolve along the  $z$ -axis. By multiplying Eq. (5) with  $\alpha_{\bar{m}}^*$  and Eq. (6) with  $\alpha_m$ , and taking into account the  $\mathcal{PT}$  symmetry of the potential  $v_m = v_{\bar{m}}^*$ , we construct the difference

$$Q_m^{(j)} - Q_{m-1}^{(j)} = (\varepsilon_j - \varepsilon_j^*) \alpha_m^{(j)} \alpha_{\bar{m}}^{*(j)}, \quad (7)$$

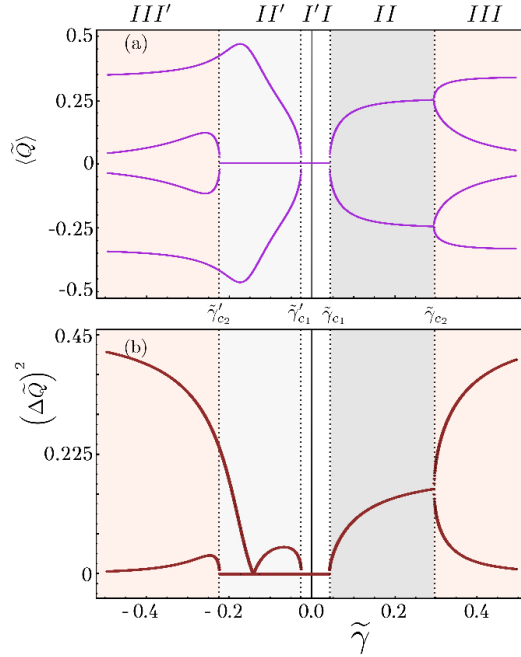


FIG. 3. (color online) (a) Phase diagram of the setup of Fig. 1 defined by the site-averaged current  $\langle \tilde{Q} \rangle$  as a function of the loss/gain parameter  $\tilde{\gamma}$ , and (b) corresponding variance  $\Delta Q^2 = \langle Q^2 \rangle - \langle Q \rangle^2$ .

with the nonlocal current of mode  $\alpha^{(j)}$  defined as

$$Q_m^{(j)} = h \left( \alpha_{m+1}^{(j)} \alpha_m^{*(j)} - \alpha_{m-1}^{*(j)} \alpha_m^{(j)} \right). \quad (8)$$

In the case of a real eigenvalue spectrum ( $\varepsilon_j = \varepsilon_j^*$ ), as in the  $\mathcal{PT}$ -symmetric phase, we obtain the equality  $Q_m^{(j)} = Q_{m-1}^{(j)}$  which signifies the spatial constancy of  $Q$ . In Ref. [27] it was shown that the corresponding quantity  $Q$  for a continuous scattering system with  $\mathcal{PT}$  symmetry is always spatially constant and becomes zero in the unbroken  $\mathcal{PT}$  phase (where the scattering states are  $\mathcal{PT}$  eigenstates). This generic spatial constancy of  $Q$  in  $\mathcal{PT}$  symmetric scattering systems stems from the fact that the energy of the incoming plane waves is taken real. Here, the eigenvalues are complex and the right hand side of Eq. (7) prevents  $Q^{(j)}$  from being spatially constant in the entire parameter space. Nevertheless, the constancy is restored in the unbroken  $\mathcal{PT}$  phase where  $\varepsilon_j = \varepsilon_j^*$ . Moreover, the restoration of global  $\mathcal{PT}$  symmetry renders  $Q$  equal to zero [27, 42]. In Ref. [27] it was indicated that, for scattering  $\mathcal{PT}$  systems,  $Q$  acts in the same way as the order parameter of a critical system, describing the transition between the  $\mathcal{PT}$  broken ( $Q \neq 0$ ) and unbroken ( $Q = 0$ ) phases. For bound systems, as the one under consideration here, the same role can be assigned to its mean value  $\langle Q \rangle$  over the lattice sites, which will be nonzero in the broken and zero in the unbroken phase. Additionally, some straightforward algebraic manipulations of Eqs. (7), (8) reveal that  $\langle Q \rangle \in \mathbb{R}$  for any number of waveguides.

Figure 3 (a) shows the four  $\langle Q^{(j)} \rangle$  (illustrated all in the same colour) with  $j = 1, 2, 3, 4$  corresponding to the

four eigenmodes of the system, as a function of  $\tilde{\gamma}$ . As expected, all four  $\langle Q^{(j)} \rangle = 0$  in the unbroken  $\mathcal{PT}$  phase (namely regions  $I'$ ,  $I$ ), while  $\langle Q^{(j)} \rangle \neq 0$  in the broken phase. The behaviour of  $\langle Q^{(j)} \rangle$  as a function of  $\tilde{\gamma}$  shares the same characteristics with  $\text{Im}[\varepsilon_j]$ , shown in Fig. 2 (a), since they exhibit the same kind of bifurcations at the same EPs  $\tilde{\gamma}_{c1}$ ,  $\tilde{\gamma}_{c2}$ . Therefore,  $\langle Q^{(j)} \rangle$  describes all the transitions of the system between phases of broken and unbroken  $\mathcal{PT}$  symmetry.

At this point, let us comment on some similarities which can be identified between the transition from the  $\mathcal{PT}$  unbroken to the  $\mathcal{PT}$  broken phase and the thermodynamic phase transition of the two-dimensional Ising model in the mean field approach. In the first place both transitions occur due to spontaneous symmetry breaking, emerging when tuning a suitable parameter (the loss/gain rate in  $\mathcal{PT}$  systems and the temperature in thermodynamics). Both cases are characterized by the existence of a quantity which is zero (nonzero) in the phase of the unbroken (broken) symmetry. In thermodynamics this quantity is the order parameter of the system (the mean magnetization  $\langle M \rangle$  for the Ising case), while in  $\mathcal{PT}$  symmetry breaking this role is assigned to  $\langle Q \rangle$ . Finally, in the vicinity of the transition points where the systems bifurcate from the unbroken to the broken phases, both  $\langle Q \rangle$  and  $\langle M \rangle$  follow a power law (which in the present case has the form  $\langle Q \rangle \sim |\tilde{\gamma} - \tilde{\gamma}_c|^{1/2}$ ) with the same exponent equal to 1/2. Equivalent power laws with exponent 1/2 occur in a multitude of scenarios involving  $\mathcal{PT}$  breaking transitions, e. g. the single dimer, a quadrimer with  $\gamma = \tilde{\gamma}$  or with  $\gamma = -\tilde{\gamma}$ . In spite of the aforementioned similarities between  $\mathcal{PT}$  symmetry breaking and continuous phase transitions, criticality is absent from  $\mathcal{PT}$  system under consideration, as indicated by the nondiverging fluctuations of  $\langle Q^2 \rangle$  at the transition points. As we see in Fig. 3 (b), the variance  $\Delta Q^2 = \langle Q^2 \rangle - \langle Q \rangle^2$  vanishes at the transition points thus rendering the character of the transition non-critical [43].

Based on Eq. (7) it is finally instructive to comment on the behaviour of the quasipower  $P_Q$  defined here as

$$P_Q = \sum_{m=1}^N \psi_m \psi_m^*. \quad (9)$$

It is well known that in nonhermitian, discrete systems the usual power oscillates along the propagation axis  $z$  [18]. On the other hand, the quasipower has been shown [6, 44] to be a conserved quantity along  $z$  in  $\mathcal{PT}$  symmetric systems for any propagating excitation (and thus zero for a single waveguide excitation), for any choice of loss/gain parameters. To study the behaviour of the quasipower of a single mode, the nonlocal current  $Q$  can be employed: Summing Eq. (7) over  $m$  ( $m = 1, \dots, 4$ , for the quadrimer case) yields

$$Q_4^{(j)} - Q_0^{(j)} = \frac{2i\text{Im}[\varepsilon_j]}{h} P_Q^{(j)}, \quad (10)$$

where  $P_Q^{(j)} = \sum_{m=1}^4 \alpha_m^{(j)} \alpha_{N+1-m}^{*(j)}$  is the quasipower of the  $j$ -th mode. Now, since  $\alpha_0 = \alpha_5 = 0$  due to the boundary

conditions, it follows that  $Q_0 = Q_4 = 0$ , showing that the quasipower for a single mode is zero—a result which holds for any number of waveguides.

#### IV. LIGHT PROPAGATION

The qualitative differences between the  $\mathcal{PT}$  unbroken and broken phases can be investigated through the light propagation in each phase. As it is expected, in the unbroken  $\mathcal{PT}$  parameter regions  $I$  and  $I'$  (real spectrum) the light propagates in the absence of attenuation or amplification, thereby oscillating among the four waveguides. Note here that, since the eigenvectors of a non-Hermitian system are not orthonormal, we use the biorthogonal basis employing the left and the right eigenvectors of  $\mathcal{H}$  [23].

##### A. Evolution of single waveguide excitation

Figure 4 (a) illustrates the propagation of light along the  $z$ -axis following a unit excitation in the second waveguide as well as the corresponding power

$$P = \sum_{m=1}^4 |\psi_m|^2. \quad (11)$$

For non-Hermitian systems the power typically oscillates along the propagation axis, with the propagation being nonreciprocal and dependent on the initially excited waveguide [31]. On the other hand, the purely imaginary spectrum in the  $\mathcal{PT}$  broken regions  $III$  and  $III'$  leads the light intensity  $\mathcal{I}$  and the power  $P$  to increase monotonously and exponentially with the propagation distance.

Of particular interest are the characteristics of the propagation in the  $\mathcal{PT}$  broken region  $II$ . For  $\tilde{\gamma}_{c_1} < \tilde{\gamma} < \tilde{\gamma}_{c_2}$  the intensity evolution is drastically altered compared to the other phases. A key characteristic of this parameter region is the exponentially growing, oscillatory pattern of the light intensity along the propagation axis. This behaviour is caused by the complex energy eigenvalues, their imaginary parts being responsible for the exponential increase and their real parts for the oscillatory behaviour. In this phase the exponential increase is much slower as compared to the phases  $III, III'$  where the eigenvalues are imaginary and of larger maximal values. This propagation pattern causes the intensity maximum to oscillate between the two gain waveguides along  $z$ , as shown in Fig. 4 (b) through a sequence of alternating intensity maxima between the 1-st and 2-nd waveguides. The effect of the complex spectrum leaves its imprints also on the power  $P$  (see inset in Fig. 4 (b)), which follows an overall exponential increase together with oscillations on a smaller scale. With the real part of the energy spectrum in this regime being doubly degenerate, those oscillations correspond to the single real energy difference yielding a period  $2\pi/\text{Re}[\bar{\epsilon}_2 - \bar{\epsilon}_1] \approx 29.64$ . As indicated in Fig. 4 (c),

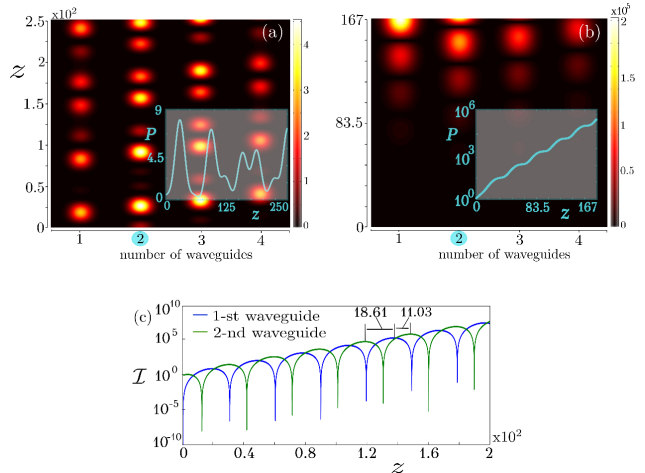


FIG. 4. (color online) Light propagation along the waveguide quadrimer for  $h = 0.1$ ,  $n = 0.1$ ,  $\gamma = 0.08$ , with light launched in the (marked) second waveguide. (a)  $\mathcal{PT}$ -symmetric phase with  $\tilde{\gamma} = 0.015$ : Intensity  $\mathcal{I}$  (color plot) and power  $P$  (inset) as a function of propagation length  $z$ . (b)  $\mathcal{PT}$  broken phase with  $\tilde{\gamma} = 0.06$ : Intensity evolution up to the length  $z = 167$  where the sixth maximum in the first waveguide occurs, and the corresponding power (inset). (c) Intensity evolution in the first and second waveguide for the parameter choice in (b): in each waveguide the maxima are equidistant with separation  $2\pi/\text{Re}[\bar{\epsilon}_2 - \bar{\epsilon}_1] \approx 29.64$ , with the maxima of the first waveguide lagging by 18.61 length units.

the oscillating pattern is also shifted by a constant length between the first and second waveguides. Note that, in the opposite parametric region  $II'$ , where the system does not exhibit complex eigenvalues, the aforementioned behaviour is not met since the purely imaginary eigenvalues dominate and lead to a clear exponential increase, similarly to regions  $III, III'$ .

##### B. Vicinity of exceptional point

Let us now look into the characteristics of the field propagation in the vicinity of the EP  $\tilde{\gamma}_{c_1} \approx 0.044$  which indicates the breaking of the  $\mathcal{PT}$  symmetry and separates region  $I$  from region  $II$  in Fig. 2. Figure 5 (a) shows the evolution of the power  $P$  along  $z$  for a range of the loss/gain parameter  $\tilde{\gamma}$  around the EP at  $\tilde{\gamma}_{c_1}$ . For a certain  $\tilde{\gamma}$  in region  $I$ , the power generally oscillates in a superposition of four different frequencies corresponding to the four absolute differences between the real energies  $\bar{\epsilon}_j$  of the spectrum. As the EP point is approached from below, the branches of the spectrum also approach each other and become pairwise double degenerate at the EP which is thus characterized by a single oscillation frequency. Marginally below the EP at  $\tilde{\gamma} = \tilde{\gamma}_{c_1} - 0.001$  we have two dominant frequencies producing a beating profile in the intensity along each waveguide as well as in the overall power. Indeed, the light intensity is characterized by revivals in each waveguide and  $P$  has two different oscillation scales. This is shown in Fig. 5 (b) for a single

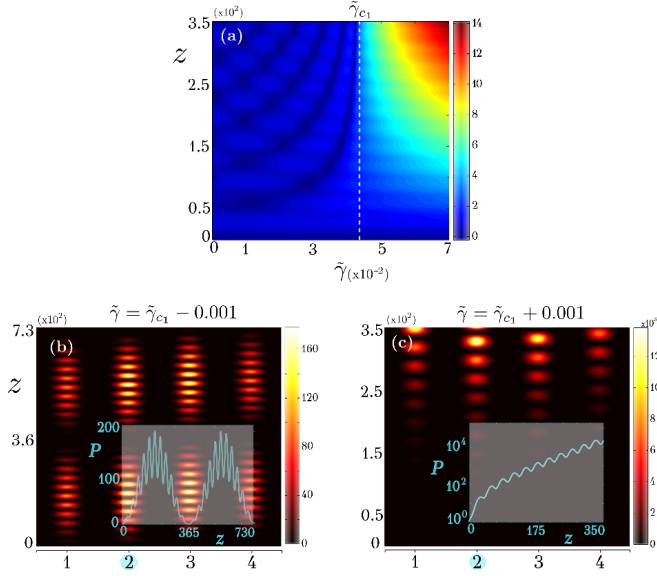


FIG. 5. (color online) (a) Power evolution as a function of the loss/gain parameter  $\tilde{\gamma}$  across the  $\mathcal{PT}$  phase transition around the exceptional point  $\tilde{\gamma}_{c1}$  (indicated by the dashed line), with intensity and power (insets) evolution shown for (b)  $\tilde{\gamma} = \tilde{\gamma}_{c1} - 0.001$  and for (c)  $\tilde{\gamma}_{c1} = \tilde{\gamma}_{c1} + 0.001$ .

waveguide excitation: The power trajectory performs fast oscillations within a slowly oscillating envelope with minima close to zero for the specific choice of parameters. As the EP is approached the envelope frequency decreases and vanishes exactly at the EP where the field intensity and the power become periodic.

Above  $\tilde{\gamma}_{c1}$  the fast oscillation persists, but the negative imaginary parts in the spectrum add an exponential increase to  $\mathcal{I}(z)$  and  $P(z)$ . When entering slightly into the broken phase of region  $II$  above  $\tilde{\gamma}_{c1}$ , the propagation is qualitatively altered due to the appearance of complex eigenvalues, as seen in Fig. 5 (c): The negative imaginary parts in the spectrum initiate an exponential increase in  $\mathcal{I}(z)$  and  $P(z)$ , while simultaneously the oscillatory behaviour is retained by the real parts. This mechanism applies throughout region  $II$ , though for larger imaginary eigenenergy parts the exponential increase completely dominates.

Finally, we note that beyond the second bifurcation point  $\tilde{\gamma}_{c2}$  both the light intensity and the power simply grow exponentially (without oscillations), similarly to the  $\mathcal{PT}$  symmetric dimer [31], due to the existence of only imaginary eigenvalues.

## V. BAND STRUCTURE AND BEAM DYNAMICS

Let us now focus on the periodic counterpart of the studied system with the quadrimer as the unit cell, that is, a lattice with period  $L = 4$ . For notational convenience the index  $m$  now enumerates the cells (i.e. the quadrimers which comprise the lattice) instead of the waveguides, and wave fields  $A_m(z)$ ,  $B_m(z)$ ,  $C_m(z)$ ,  $D_m(z)$  are assigned

(from the left) to the waveguides of the  $m$ -th unit cell. Using the coupled mode approximation we arrive at the following four equations describing the evolution of the fields along the  $z$ -axis:

$$\begin{aligned} i \frac{dA_m(z)}{dz} &= v A_m(z) + \eta D_{m-1}(z) + h B_m(z) \\ i \frac{dB_m(z)}{dz} &= \tilde{v} B_m(z) + h A_m(z) + h C_m(z) \\ i \frac{dC_m(z)}{dz} &= \tilde{v}^* C_m(z) + h B_m(z) + h D_m(z) \\ i \frac{dD_m(z)}{dz} &= v^* D_m(z) + h C_m(z) + \eta A_{m+1}(z), \end{aligned} \quad (12)$$

where  $v$ ,  $\tilde{v}$  are the on-site potentials and  $h$ ,  $\eta$  are the intra- and inter-cell hoppings, respectively. To obtain the band structure of the system we use the Fourier transform of the fields in the first Brillouin zone (BZ), e.g.  $A_m(z) = \frac{1}{2\pi} \int_{-\pi/L}^{\pi/L} \tilde{A}_k e^{ikLm} dk$ , and write Eqs. (12) in matrix notation as  $i \frac{d}{dz} |\tilde{\Psi}_k\rangle = \hat{\mathcal{H}}_k |\tilde{\Psi}_k\rangle$  with

$$|\tilde{\Psi}_k\rangle = \begin{pmatrix} \tilde{A}_k(z) \\ \tilde{B}_k(z) \\ \tilde{C}_k(z) \\ \tilde{D}_k(z) \end{pmatrix}, \quad \hat{\mathcal{H}}_k = \begin{pmatrix} v & h & 0 & \eta e^{-ikL} \\ h & \tilde{v} & h & 0 \\ 0 & h & \tilde{v}^* & h \\ \eta e^{ikL} & 0 & h & v^* \end{pmatrix}. \quad (13)$$

The on-site potentials remain the same as in Eq. (3). The four eigenvalues  $\varepsilon_j(k)$  of  $\hat{\mathcal{H}}_k$  provide the dispersion relation for the system, implying the existence of four bands.

Figure 6 (a), (b) illustrates the real and imaginary parts of the dispersion relation  $\varepsilon_j(k)$  as a function of the loss/gain parameter  $\tilde{\gamma}$ . The remaining parameters are kept fixed with the values  $n = 0.1$ ,  $h = \eta = 0.1$  and  $\gamma = 0.01$ . As we see, the bands have imaginary branches for any  $\tilde{\gamma} \neq 0$ , indicating the general absence of a  $\mathcal{PT}$  symmetric phase for this parameter choice. Note that the absence of a  $\mathcal{PT}$  symmetric phase is general for the choice of uniform  $h = \eta$  inter and intra cell hoppings. However, the width of the  $k$ -regions with  $\text{Im}[\varepsilon_j(k)] = 0$  depend strongly on  $\tilde{\gamma}$ . Indeed, the enriched dispersion relation induced by the loss/gain parameter competition offers an additional degree of freedom regarding the manipulation of the size of the  $k$ -regions with real energy eigenvalues. In particular, the interplay of  $\gamma$ ,  $\tilde{\gamma}$  causes the coexistence of  $k$ -regions with  $\text{Im}[\varepsilon_j] \neq 0$  around the centre and at the edges of the BZ for small  $\tilde{\gamma}$ . In the vicinity of  $\tilde{\gamma} = 0$  real energies dominate, while  $\text{Im}[\varepsilon_j] \neq 0 \forall k \in [-\pi/4, \pi/4]$  for values larger than  $\tilde{\gamma} \simeq 0.19$ . Note that for  $\gamma = \tilde{\gamma}$  ( $\gamma = -\tilde{\gamma}$ ) complex energy regions appear only at the edges (centre) of the BZ (see inset in Fig. 6).

The occurrence of  $k$ -regions with complex band branches at the centre and edges of the BZ, combined with their size dependence on  $\tilde{\gamma}$ , provides a flexible way to design wavepackets which can travel varying propagation distances before the exponential intensity growth starts. The distance  $z_L$  where the divergence begins (which we define by the doubling of optical power,  $P(z_L) \equiv 2P(0)$ ) depends strongly on how well localized the wavepacket is around the initial momentum  $p_0$ , and in turn whether it

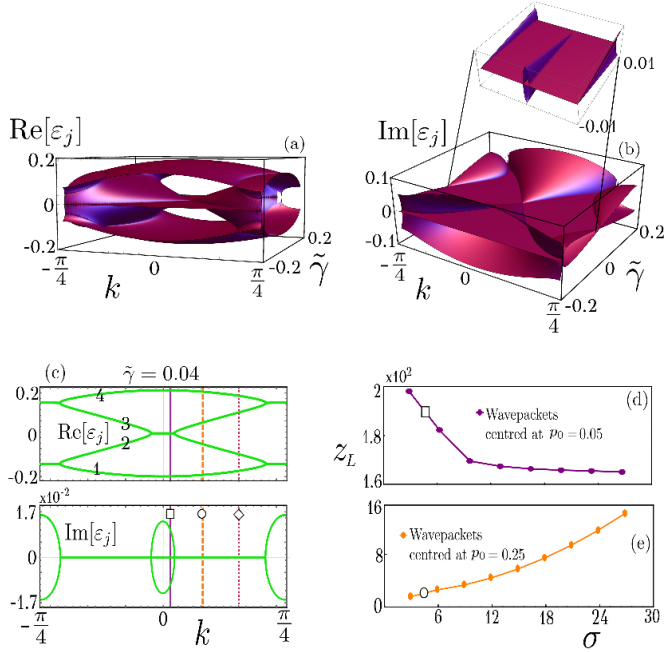


FIG. 6. (color online) (a) Real and (b) imaginary parts of the dispersion relation  $\varepsilon_j(k)$  of the periodic waveguide array with quadrimer unit cell as a function of the loss/gain parameter  $\tilde{\gamma}$ , for  $n = 0.1$ ,  $h = \eta = 0.1$  and  $\gamma = 0.01$ . The inset shows the band structure around zero, elucidating the cases  $\tilde{\gamma} = \gamma$  and  $\tilde{\gamma} = -\gamma$ . (c) Band structure for  $\tilde{\gamma} = 0.04$  (indicated by the green line in (b)). The numbers enumerate the four bands. (d,e) Propagation length  $z_L$  up to power divergence (defined by  $P(z_L) \equiv 2P(0)$ ) for varying width  $\sigma$  of a Gaussian wavepacket launched at the center of the array with initial momentum (d)  $p_0 = 0.05$  and (e)  $p_0 = 0.25$ .

is localized around Bloch wavenumbers  $k$  with real dispersion or not. As seen in Fig. 6 (b), the latter can be engineered in the presence of the additional loss/gain parameter. To elaborate on this concept via an exemplary case we focus on the band structure for  $\tilde{\gamma} = 0.04$ , shown in Fig. 6 (c), with complex band branches around the center ( $|k| \lesssim 0.075$ ) and edges ( $|k| \gtrsim 0.66$ ). At the same time, we consider a Gaussian wavepacket  $A(n; 0) = (\sqrt{\pi} \sqrt{\sigma})^{-1} e^{ip_0 n} e^{-i(n-n_0)^2/2\sigma^2}$  with initial momentum  $p_0 = 0.05$  launched at the center ( $n_0 = 200$ ) of a finite periodic array of  $N = 100 \times 4$  waveguides. The array is chosen large enough to enable a connection between the basic wavepacket propagation properties and the features of the given band structure.

Remarkably, the wavepacket can indeed travel a long distance  $z_L$  without diverging, even though the unbroken  $\mathcal{PT}$ -symmetric phase is overall absent in the band structure. In other words, propagation properties which would be expected only in the  $\mathcal{PT}$  symmetric phase of a setup may also be encountered as transient phenomena in the much larger parameter regions of  $\mathcal{PT}$  broken phases. This situation is illustrated in Fig. 6 (d,e) which shows the distance  $z_L$  for a Gaussian wavepacket as a function of its width  $\sigma$ , for different initial momenta  $p_0$ . For a small momentum  $p_0 = 0.05$ , the distance  $z_L$  decreases

with increasing  $\sigma$  (Fig. 6 (d)). In contrast, for a moderate momentum  $p_0 = 0.25$  the propagation distance pattern is reversed, with  $z_L$  now increasing with  $\sigma$  (Fig. 6 (e)).

In order to understand this behavior, we analyze the contribution of real and imaginary eigenvalue branches in the band structure of the periodic counterpart to the initial wavepacket, given its initial width. Since the associated Bloch momenta are not conserved in the finite periodic setup, the decomposition of the wavepacket in  $k$ -space will evolve in time, thus eventually extending to other regions in the BZ. If the wavepacket is spatially broad and strongly localized in  $k$ -space, the dispersion (Fig. 6 (c)) suggests that it will diverge after a relatively long (short) propagation distance  $z_L$  when it is initially localized in a  $k$ -region without (with)  $\text{Im}[\varepsilon_j(k)] > 0$ . The contribution of  $k$ -values to the wavepacket is here determined by the magnitude of its expansion coefficients  $c_j(k)$  in the space of corresponding right Bloch eigenstates (with periodic parts given by the right eigenvectors of  $\hat{\mathcal{H}}_k$ ), that is, its projection on left Bloch eigenstates [44]. The wavepacket of Fig. 6 (d) starts with a momentum  $p_0$  lying in the central complex region of the band structure (solid vertical line in Fig. 6 (c)), and thereby diverges rapidly for large width  $\sigma$  (strong  $k$ -localization). When  $\sigma$  is decreased, the (biorthogonally normalized)  $|c_j(k)|^2$  are depleted in the region of complex  $\varepsilon_j(k)$  and extend increasingly into real regions, so that the divergence of the wavepacket is delayed and  $z_L$  increases. On the contrary, the wavepacket of Fig. 6 (e) with larger  $p_0$  (dashed vertical line in Fig. 6 (c)) is initially localized in  $k$ -space in real dispersion regions. It therefore shows longer stable propagation for large  $\sigma$ , with  $z_L$  decreasing when the initial wavepacket delocalizes in  $k$ -space into the complex dispersion regions (with  $\text{Im}[\varepsilon_j(k)] < 0$ ).

To illustrate this mechanism in the beam dynamics, we show in Fig. 7 (a) the intensity evolution of a relatively broad wavepacket ( $\sigma = 13$ ) with initial momentum  $p_0 = \pi/9$  (indicated by the dotted vertical line in the band structure of Fig. 6 (c)) up to the length of power divergence (as depicted in the inset) together with its Bloch state coefficients  $|c_j(k)|^2$  in each band  $j$  in Fig. 7 (b). Upon its launching, the wavepacket is split into four beams of different intensities, with slopes corresponding to the group velocities of (the real parts of) the dispersion regions populated in each of the four bands. One main beam is enhanced in intensity, which is reflected also in its  $k$ -space decomposition in the first band. After some propagation distance ( $z \gtrsim 400$ ) the light field starts populating Bloch momenta in the  $k$ -regions with complex band branches. In particular, the region with  $\text{Im}[\varepsilon_1(k)] < 0$  (of band  $j = 1$ ) at the lower edge of the BZ is increasingly populated with  $z$ , as indicated by the arrows in Fig. 7 (b), thus leading to exponential divergence of the light intensity in the corresponding  $k$ -space contribution. Since the profile of this monotonically increasing part of  $|c_1(k)|^2$  is narrow and localized at a practically flat  $\text{Re}[\varepsilon_1(k)]$  dispersion region (see lower BZ edge in Fig. 6 (c)), the corresponding real space evolution will be a very broad, exponentially increasing beam in forward direction (zero group velocity)—indeed, this exponential

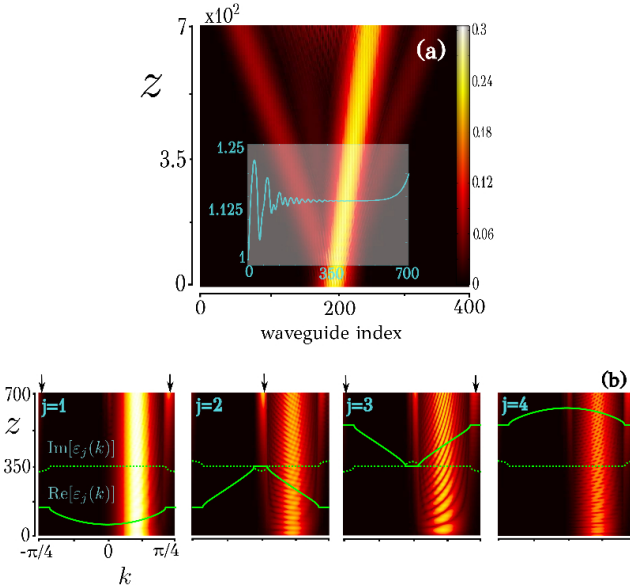


FIG. 7. (color online) Propagation of a Gaussian wavepacket of width  $\sigma = 13$  launched from the center of an array of  $N = 400$  waveguides with initial momentum (a)  $p_0 = \pi/9$  and the corresponding optical power evolution  $P(z)$  (inset). (b) Expansion coefficients  $|c_j(k)|^2$  in the right Bloch states of the corresponding periodic system, in each of the four bands  $j = 1, 2, 3, 4$ , for the wavepacket in (a). The green dashed (solid) lines show the imaginary (real) part of each band multiplied by  $1.5 \times 10^3$ . The arrows indicate the gradual population of the regions with  $\text{Im}[\varepsilon_j(k)] < 0$ , causing the exponential increase.

increase begins to become visible at the top of the intensity evolution in Fig. 7(a). Note, that any stationary mode with energy eigenvalue  $\varepsilon_j$  evolves in  $z$  with a phase factor  $e^{i\varepsilon_j z}$ .

The above analysis demonstrates that  $\mathcal{PT}$ -symmetric periodic lattices can be designed for quasistable propagation of appropriately launched wavepackets even in the  $\mathcal{PT}$ -broken phase of the stationary dynamics, parametrically tunable in terms of different loss/gain parameters.

## VI. CONCLUDING REMARKS

In this work we analyzed a discrete  $\mathcal{PT}$  symmetric optical system, comprised of four waveguides with two competing loss/gain parameters  $\gamma$  and  $\tilde{\gamma}$ . The addition of  $\tilde{\gamma}$  is shown to have a major impact on the structure of the

phase diagram of the system, giving rise not only to transitions between unbroken and broken  $\mathcal{PT}$  phases, but also between qualitatively different  $\mathcal{PT}$  broken phases.

We have shown also the existence of a  $\mathcal{PT}$  symmetry induced current  $Q$  which becomes zero (and constant) in the  $\mathcal{PT}$  symmetric phase. The mean value  $\langle Q \rangle$  describes the transition between the phases of unbroken ( $\langle Q \rangle = 0$ ) and broken ( $\langle Q \rangle \neq 0$ ) symmetry. This finding is in agreement with the continuous version of  $Q$  [27] that describes the transition of  $\mathcal{PT}$  symmetry breaking and generalizes the phase diagram for  $\mathcal{PT}$  scattering systems. Hence,  $\langle Q \rangle$  can be considered as the natural “order parameter” for the symmetry breaking in the generic class of  $\mathcal{PT}$  symmetric systems (discrete, continuous, bounded or scattering).

The investigation of light propagation with a particular focus on the  $\mathcal{PT}$  broken phase characterized by complex eigenvalues, revealed interesting properties such as exponentially growing oscillations of the intensity maximum between the gain waveguides. Employing then the quadrimer as a unit cell, we obtained the band structure for the corresponding infinite system. The additional loss/gain parameter  $\tilde{\gamma}$  enriches significantly the eigenvalue landscape, giving rise to additional  $k$ -space regions which correspond to complex eigenvalues. The extent of these regions is shown to be varying with respect to  $\tilde{\gamma}$ . Finally, employing a Bloch mode analysis and guided by the imaginary part of the band structure, we showed how a wavepacket can be designed in order to control its propagation distance before starting to diverge. This offers the possibility to observe propagation properties which are accessible in the  $\mathcal{PT}$  symmetric phase, in the -parametrically much larger- broken phases.

Further studies of extended lattices with  $\mathcal{PT}$  symmetry and competing loss/gain rates are expected to provide a deeper understanding on how the band structure and the attendant beam dynamics are affected. Particularly, the interplay between competing loss/gain and different hoppings could be expected to influence significantly the beam propagation properties in suitably designed waveguide arrays.

## VII. ACKNOWLEDGEMENTS

P.A.K acknowledges financial support from IKY Fellowships of Excellence for Postdoctoral Research in Greece - Siemens Program.

---

[1] C. M. Bender, D. C. Brody, and H. F. Jones, Phys. Rev. Lett. **89**, 270401 (2002).  
[2] C. M. Bender, D. C. Brody, and H. F. Jones, Phys. Rev. D **70**, 025001 (2004).  
[3] H. Schomerus, Opt. Lett. **38**, 1912 (2013).  
[4] B. Zhu, R. Lü, and S. Chen, Phys. Rev. A **89**, 062102 (2014).  
[5] C. Poli, M. Bellec, U. Kuhl, F. Mortessagne, H. Schomerus, Nat. Commun. **6**, 062102 (2015).  
[6] R. El-Ganainy, K. G. Makris, D. N. Christodoulides and Z. H. Musslimani, Opt. Lett. **32**, 2632 (2007).  
[7] K. G. Makris, R. El-Ganainy, D. N. Christodoulides and Z. H. Musslimani, Phys. Rev. A **81**, 063807 (2010).  
[8] Z. H. Musslimani, K. G. Makris, R. El-Ganainy, and D. N. Christodoulides, Phys. Rev. Lett. **100**, 030402 (2008);

[9] Z. H. Musslimani, K. G. Makris, R. El-Ganainy, and D. N. Christodoulides, *J. Phys. A* **41**, 244019 (2008).

[10] B. Peng, S. K. Özdemir, F. Lei, F. Monifi, M. Gianfreda, G. L. Long, S. Fan, F. Nori, C. M. Bender and L. Yang, *Nat. Phys.* **10**, 394 (2014).

[11] C. M. Bender, M. Gianfreda, S. K. Özdemir, B. Peng, and L. Yang, *Phys. Rev. A* **88**, 062111 (2013).

[12] X. Zhu, H. Ramezani, C. Shi, J. Zhu, and X. Zhang, *Phys. Rev. X* **4**, 031042 (2014).

[13] X. Zhu, H. Ramezani, C. Shi, J. Zhu, and X. Zhang, *J. Acoust. Soc. Am.* **137**, 2403 (2015).

[14] R. Fleury, D. Sounas, and A. Alú, *Nat. Comm.* **6**, 5906 (2015).

[15] C. M. Bender and S. Boettcher, *Phys. Rev. Lett.* **80**, 5243 (1998).

[16] C. E. Rüter, K. G. Makris, R. El-Ganainy, D. N. Christodoulides, M. Segev and D. Kip, *Nat. Phys.* **6**, 192 (2010).

[17] A. Guo, G. J. Salamo, D. Duchesne, R. Morandotti, M. Volatier-Ravat, V. Aimez, G. A. Siviloglou, and D. N. Christodoulides, *Phys. Rev. Lett.* **103**, 093902 (2009).

[18] K. G. Makris, R. El-Ganainy, D. N. Christodoulides and Z. H. Musslimani, *Phys. Rev. Lett.* **100**, 103904 (2008).

[19] H. Ramezani, T. Kottos, R. El-Ganainy, and D. N. Christodoulides, *Phys. Rev. A* **82**, 043803 (2010).

[20] J. D'Ambroise, P. G. Kevrekidis, and S. Lepri, *J. Phys. A* **45**, 444012 (2012).

[21] F. Yang and Z. L. Mei, *Sci. Rep.* **5**, 14981 (2015).

[22] S. Longhi, *Phys. Rev. Lett.* **103**, 123601 (2009).

[23] M. C. Zheng, D. N. Christodoulides, R. Fleischmann and T. Kottos, *Phys. Rev. A* **82**, 010103(R) (2010).

[24] A. Ruschhaupt, F. Delgado, and J. G. Muga, *J. Phys. A* **38**, 171 (2005).

[25] Y. D. Chong, L. Ge, and A. D. Stone, *Phys. Rev. Lett.* **106**, 093902 (2011).

[26] L. Ge, Y. D. Chong, and A. D. Stone, *Phys. Rev. A* **85**, 023802 (2012).

[27] P. A. Kalozoumis, G. Pappas, F. K. Diakonos and P. Schmelcher, *Phys. Rev. A* **90**, 043809 (2014).

[28] P. Ambichl, K. G. Makris, L. Ge, Y. D. Chong, A. D. Stone, and S. Rotter, *Phys. Rev. X* **3**, 041030 (2013).

[29] R. L. Horne, J. Cuevas, P. G. Kevrekidis, N. Whitaker, F. Kh. Abdullaev, and D. J. Frantzeskakis, *J. Phys. A* **46**, 485101 (2013).

[30] K. Li and P. G. Kevrekidis, *Phys. Rev. E* **83**, 066608 (2011).

[31] T. Kottos, *Nat. Phys.* **6**, 166 (2010).

[32] K. Li, P. G. Kevrekidis, D. J. Frantzeskakis, C. E. Rüter and D. Kip, *J. Phys. A* **46**, 375304 (2013).

[33] D. A. Zezyulin and V. V. Konotop, *Phys. Rev. Lett.* **108**, 213906 (2012).

[34] V. V. Konotop, D. E. Pelinovsky and D. A. Zezyulin, *Europhys. Lett.* **100**, 56006 (2012).

[35] S. K. Gupta and A. K. Sarma, *J. Mod. Opt.* **61**, 227 (2014).

[36] S. K. Gupta, J. P. Deka and A. K. Sarma, *Eur. Phys. J. D* **69**, 199 (2015).

[37] S. Phang, A. Vukovic, S. C. Creagh, P. D. Sewell, G. Gradoni, T. M. Benson, arXiv:1507.06699v1.

[38] P. A. Kalozoumis, C. Morfonios, F. K. Diakonos and P. Schmelcher, *Phys. Rev. Lett.* **113**, 050403 (2014).

[39] P. A. Kalozoumis, C. Morfonios, N. Palaiodimopoulos, F. K. Diakonos, and P. Schmelcher, *Phys. Rev. A* **88**, 033857 (2013).

[40] P. A. Kalozoumis, C. Morfonios, F. K. Diakonos, and P. Schmelcher, *Ann. Phys.* **362**, 684 (2015).

[41] P. A. Kalozoumis, C. Morfonios, F. K. Diakonos, and P. Schmelcher, *Phys. Rev. A* **87**, 032113 (2013).

[42] C. Morfonios, P. A. Kalozoumis, F. K. Diakonos, and P. Schmelcher, in preparation.

[43] N. Goldenfeld, *Lectures On Phase Transitions And The Renormalization Group (Frontiers in Physics)*, (Addison-Wesley Publishing Company, New York) (1992).

[44] K. G. Makris, R. El-Ganainy, D. N. Christodoulides and Z. H. Musslimani, *Int. J. Theor. Phys.* **50**, 1019 (2011).